7 - 12 SEPTEMBER 2014, KRAKÓW
FORUM ACUSTICUM

Time-domain simulations of low-height porous noise barriers with periodically spaced scattering inclusions

Bart van der Aa & Jens Forssén
Department of Civil and Environmental Engineering, Division of Applied Acoustics, Chalmers University of Technology, SE-41296 Göteborg, Sweden.

Summary
In this work we investigate the possibility to create a noise reducing device by embedding periodically spaced scattering units into a porous matrix. A numerical study based on the Finite-Difference Time-Domain method is therefore performed. The porous matrix is modelled by the Zwikker and Kosten phenomenological porous rigid-frame model, and scattering units are considered to be acoustically rigid. For simplicity a two-dimensional computational domain and a homogeneous atmosphere has been assumed. We focus on low-height noise barriers with the intention to reduce traffic noise alongside pavements, e.g. for pedestrians and cyclists. A number of porous barriers with acoustically rigid inclusions are investigated and compared against porous barriers without scattering units added. In addition, the reduction is tested against a simple acoustically rigid screen.

1. Introduction

Noise pollution is a major environmental problem in Europe and even more substantial on a global scale. The social cost of traffic noise has been estimated to 0.4% of the total Gross Domestic Product (GDP) for the European Union, and the main contribution is due to road traffic noise [1]. Mitigation and control of outdoor traffic noise in urban areas is therefore an issue of high need, both at present and in the future.

In urban areas, or more specifically city centres, busy roads often run parallel to pavements, cycle lanes, or park areas. Acoustic measures to reduce noise impact for pedestrians and cyclists recreating or commuting in these exposed zones are usually accepted up to a height of approximately 1 m. This class of noise reducing devices, here referred to as low-height noise barriers, have been studied by several authors, see e.g. [2, 5, 9]. In brief, they concluded that replacing a rigid low-height barrier with one having an effective finite surface-impedance, or a sound-permeable porous structure, can significantly improve the noise reducing performance. In addition, it can be envisioned that noise barriers in city environments shall benefit from partial absorption of the incoming wave-field, as to reduce multiple reflections between barrier and sound source, or barrier and buildings.

In recent work, it has been shown that the absorptive properties of a layer of porous material with or without rigid backing can be enhanced by including a set of scattering units in the porous matrix [3, 4, 6, 7]. The presence of periodically spaced scattering units in a matrix of porous material may give rise to energy entrapment, which is linked to (trapped) mode excitation [4]. Experimental, theoretical and numerical studies on these hybrid materials have been performed, though mostly using a type of foam as host material, which is not durable in an outdoor environment.

In this work a number of porous low-height noise barriers with rigid inclusions will be studied. The aim is (i) to design a structure with improved absorptive properties compared to a porous structure without scattering inclusions, and (ii) to design a noise reducing device effective for nearby pedestrians and cyclists. A porous material manufactured from recycled glass granular, produced by Z-block Norden AB in Sweden, is chosen as host material. The inclusions are either square or U-shaped rigid objects, the latter type with various possibilities for opening orientations. Barriers with and without rigid backing are considered and compared against a simple rigid screen of the same height and width. We will, however, first investigate absorption and transmission loss properties of the composite material, for plane wave excitation.

2. The model

Acoustic wave propagation in two-dimensional outdoor configurations is modelled using the Finite-Difference Time-Domain (FDTD) method. The FDTD method relies on spatial and temporal discretisation of the acoustic wave equation, and therefore allows us to study complex configurations such as porous noise barriers with acoustically rigid scattering inclusions of arbitrary shape. The basic equations, selected discretisation schemes, domain termination and other implementation considerations are described in the following subsections.

2.1. Sound propagation in air

Acoustic wave propagation through air can be described using the linearised Euler equations [8],

$$\frac{\partial p}{\partial t} = -\kappa \nabla \cdot \mathbf{u} + \kappa Q, \tag{1}$$

and

$$\frac{\partial \mathbf{u}}{\partial t} = -\frac{\nabla p}{\rho_0}, \tag{2}$$

where, $\mathbf{x} = (x, z) \subset \mathbb{R}^2$, $p(\mathbf{x}, t)$ is the pressure field, $\mathbf{u} = [(u(\mathbf{x}, t), w(\mathbf{x}, t)]$ is the velocity field, $Q(\mathbf{x}, t)$ the mass source term and $\kappa = \rho_0 c_0^2$ is the adiabatic bulk modulus, in which ρ_0 and c_0 are the air density and adiabatic sound speed of air, respectively. In component form and two spatial dimensions, Eq. 1 and Eq.2 are given by:

$$\frac{\partial p}{\partial t} = -\kappa \left(\frac{\partial u}{\partial x} + \frac{\partial w}{\partial z} \right) + \kappa Q, \tag{3}$$

$$\frac{\partial u}{\partial t} = -\frac{1}{\rho_0} \frac{\partial p}{\partial x}, \tag{4}$$

$$\frac{\partial w}{\partial t} = -\frac{1}{\rho_0} \frac{\partial p}{\partial z}. \tag{5}$$

These equations can be solved, e.g. using centred difference approximations of the spatial and temporal derivatives. We consider a spatially staggered finite-difference grid where the pressures are sampled at integer nodes, $x = i\Delta x$ and $z = i\Delta z$. The velocity components are spatially staggered with half a step size from the pressure nodes, i.e. u by $\Delta x/2$ and w by $\Delta z/2$. A time advancing scheme using centred finite differences over two time-steps as suggested in [8] has been used. Our program is therefore explicitly second-order accurate in both the spatial and the temporal dimensions.

2.2. Sound propagation in porous media

Sound propagation in porous media is here simulated according to the Zwikker and Kosten phenomenological model, which is given by [12]:

$$\frac{\partial p}{\partial t} = -\frac{\kappa \nabla \cdot \mathbf{u}}{\Omega k_s}, \tag{6}$$

and

$$\frac{\partial \mathbf{u}}{\partial t} = -\frac{\nabla p \Omega}{\rho_0 k_s} - \frac{\sigma \Omega}{\rho_0 k_s}, \tag{7}$$

where, σ is the flow resistivity of the porous medium, k_s the structure factor, and Ω the porosity. Using these equations sound propagation through a rigid-frame porous medium is well described, and seems a logical choice for the application at hand. For later convenience we formulate matching frequency domain solutions of the Zwikker and Kosten time-domain model. Assuming a $e^{-i\omega t}$ time convention, the normalised characteristic impedance of the material may be written [10]:

$$Z = \sqrt{\frac{i\sigma}{\rho_0 \omega \Omega} + \frac{k_s}{\Omega^2}}, \tag{8}$$

and the complex wavenumber,

$$\Gamma = \frac{\omega}{c_0} \sqrt{\frac{i\sigma\Omega}{\rho_0 \omega} + k_s}. \tag{9}$$

2.3. Perfectly matched layer

To eliminate spurious reflections from open domain terminations a Perfectly Matched Layer (PML) is commonly used, and has been proven to be a good performing absorbing layer for acoustic waves [11]. The advantage of a PML over a traditional Absorbing Boundary Layer (ABL) is that the layer is operating on both the normal components of the pressure and the velocity, which means that the layer is effective for all angles of incidence. The linearised equations for a non-moving medium with PML can be written [11]:

$$\frac{\partial p}{\partial t} = -\kappa \nabla \cdot \mathbf{u} - \alpha(\mathbf{x}) p, \tag{10}$$

$$\frac{\partial \mathbf{u}}{\partial t} = -\frac{\nabla p}{\rho_0} - \alpha(\mathbf{x}) \mathbf{u}, \tag{11}$$

where, α is the attenuation coefficient, which is zero or positive inside the PML region. Following Berenger's original formulation for electromagnetic problems, the pressure field has been split into components parallel and perpendicular to the PML. Consequently, $p =$

$p_x + p_z$, and for two spatial dimensions a set of four update equations are to be solved within the PML:

$$\frac{\partial p_x}{\partial t} = -\kappa \frac{\partial u}{\partial x} - \alpha_x p_x, \tag{12}$$

$$\frac{\partial p_z}{\partial t} = -\kappa \frac{\partial w}{\partial z} - \alpha_z p_z, \tag{13}$$

$$\frac{\partial u}{\partial t} = -\frac{1}{\rho_0} \frac{\partial p}{\partial x} - \alpha_x u, \tag{14}$$

$$\frac{\partial w}{\partial t} = -\frac{1}{\rho_0} \frac{\partial p}{\partial z} - \alpha_z w. \tag{15}$$

Time advancement of Eq. 12 – 15, in the PML region, is done using exponential differentiation, as described in e.g. [11]. Important for the performance of the PML are the attenuation coefficients. A stable and well performing scheme is to gradually increase the damping coefficients according to,

$$\alpha_x = \beta \left(\frac{x - x_{PML}}{D} \right)^m, \tag{16}$$

where $x - x_{PML}$ is the location in the PML layer, D the thickness of the layer, β the maximum amplitude of α and m is a coefficient. The parameters as discussed are set to $D = 40\Delta x$ m, $\beta = 1e6$ $1/s$ and $m = 2$.

2.4. Simulation parameters and numerical validation

Throughout the paper a spatial grid-cell spacing of $\Delta x = \Delta z = 0.0025$ m, has been used. We will consider frequencies up to 5 kHz, which corresponds to approximately 16.4 grid points per wavelength for the porous medium (the slowest medium) and about 27.5 points per wavelength in air. For numerical stability, the spatial grid spacing $\Delta r = 1/\sqrt{(\Delta x)^{-2} + (\Delta z)^{-2}}$ and the time-step Δt must be chosen such that, $C < 1/\sqrt{2}$, see e.g. [8], where the Courant number

$$C = \frac{c\Delta t}{\Delta r}, \tag{17}$$

in which, c the propagation speed of the medium. Setting the Courant number to 0.5 thus results in a time resolution of $\Delta t = 2.5e-6$ s, and about 58000 time steps for 0.15 s of simulated propagation, which was needed for a pulse to escape the computational domain completely. The source signal is a Gaussian pulse, given by:

$$Q = Ae^{-\pi^2 f_c^2 (t-t_c)^2}, \tag{18}$$

where, the amplitude A is set to unity, the centre-frequency f_c is set to 3 kHz and $t_c = 100\Delta t$.

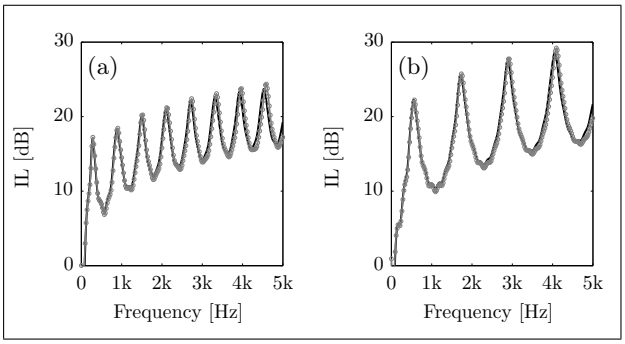

Figure 1. Narrowband insertion loss spectra for a thin 1 m tall acoustically rigid screen. For both plots we have, *thick-black*: FDTD, and *grey, open circles*: BEM using 20 points per wavelength. (a): IL at (x_r, z_r) = (5 m, 1.5 m), and (b): IL at (x_r, z_r) = (10 m, 1.5 m).

Validation of the developed program and selected parameters is done, numerically, by comparing the insertion loss spectra of a thin rigid screen computed with FDTD and the Boundary Element Method (BEM). Insertion losses are calculated according to:

$$IL = 20 \log_{10} \frac{|p_{ref}|}{|p_{tot}|}, \tag{19}$$

where, p_{tot} captures the total pressure field, and p_{ref} the reference field. The height of the screen is set to 1 m, whereas the width spans over one FDTD grid-cell, i.e. 0.0025m. The lower-left corner of the barrier is seen as the origin of the domain, and a coherent noise source is placed at (x_s, z_s) = (-2 m, 0.001 m). The methods are compared for two receiver locations, placed at (x_r, z_r) = (5 m, 1.5 m) and (x_r, z_r) = (10 m, 1.5 m). Results are shown in Fig. 1. It can be seen that the agreement between the methods is good, for both receiver locations, and all frequencies. It may, however, be observed that, the spectral agreement does gradually decrease with frequency due grid-dispersion. Although this could be reduced, e.g by implementating higher order finite-difference schemes, it is not considered in the work presented here.

3. Normal incidence sound absorption and transmission loss of a porous matrix with rigid inclusions

In the following section, we will study normal incidence sound absorption and transmission loss characteristics of a porous matrix with periodically spaced rigid inclusions. The type of inclusions considered are closed squares and open U-shape scatterers, where the latter type can have various opening orientations. For normal (plane wave) incidence only one section, or unit-cell needs to be modelled perpendicular to the direction of propagation. That is, a periodic pattern is

Figure 2. Sample (10 cm in diameter) of recycled glass granular, manufactured by Z-block Norden AB. The sample is 5.25 cm thick.

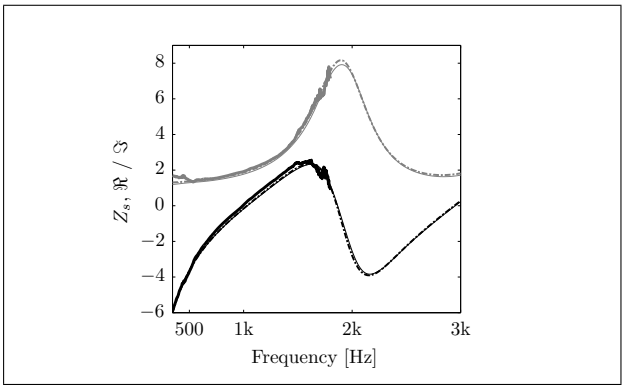

Figure 3. Surface impedance Z_s of a 5.25 cm thick recycled glass granular sample, with rigid backing. Depicted are: *grey*: $\Re(Z_s)$; *black*: $\Im(Z_s^*)$; *thick line*: measurements; *dash-dot-dash*: fitted predictions, and *thin line*: FDTD calculations.

created when domain-ends perpendicular to the incident wave are terminated with a zero-velocity boundary condition. We start, however, by obtaining acoustic properties of a porous material being applicable in outdoor environments.

3.1. Model parameter fitting of the porous material

As a starting point, a 5.25 cm thick porous material manufactured from recycled glass granular is used, see Fig. 2. In order to characterise this material using the rigid-frame porous model, σ, k_s and Ω of the sample needs to be obtained.

Finding these parameters of the sample material can be done by fitting the theoretical surface impedance of a porous layer with rigid backing against the measured surface impedance, obtained through impedance tube measurements. Generally, the acoustical surface impedance of a test material is given by

$$Z_s = Z_0 \frac{1+R}{1-R}, \tag{20}$$

where, R is the complex reflection factor at the surface of the test material and Z_0, the characteristic impedance of air. A standard transfer function method is used to compute R. The impedance tube has an inner diameter of 10 cm, holds test samples of thickness, $d = 5.25$ cm, and uses a microphone switching technique (a single microphone is used to measure the transfer function). The surface impedance as given in Eq. 20 is generally applicable for any type of sample mounting condition. However, in case of a porous layer with a rigid backing, the surface impedance may be written as follows:

$$Z_s = Z \coth(-i\Gamma d). \tag{21}$$

Now, minimising the least squares error between Eq. 20 and Eq. 21 by varying σ, k_s and Ω, we can find the best fit of these parameters. The obtained parameters, $\sigma = 29.6$ kPa s m^{-2}, $k_s = 2.84$ and $\Omega = 0.45$ are then, in turn, used as model input in the FDTD calculations. Note that, the measured data for parameter fitting has been restricted to a frequency range from 340 to 1800 Hz. The fitted, measured, and FDTD computed Z_s curves are shown in Fig. 3. As can be seen, the agreement is very good, both in terms of $\Re(Z_s)$ and $\Im(Z_s)$.

3.2. Normal incidence sound absorption and transmission loss

The normal incidence sound absorption and transmission loss of a mono (5.25 cm) and double (10.5 cm) layer porous material, with or without rigid backing will be considered. The porous sample-height has in all cases been fixed to 5.25 cm. Scattering inclusions with a fixed side-length of 2.75 cm are added in the porous matrix, and positioned in the centre of the unit cell(s). Other inclusion side-lengths have also been studied, though are omitted for brevity. The inclusions are either closed squares □, or U-shaped scatterers with the opening side(s) facing left ⊐, right ⊏ or upwards ⊔. For the latter class of scatterers a flange thickness of 0.0025 m has been modelled, which corresponds to one grid-cell. All scatterers are assumed to have perfectly reflecting surfaces, i.e. the velocity in normal direction has been set to zero. The normal incidence sound absorption and transmission loss coefficients are obtained on the surface of the porous layer, and computed through conservation of energy, i.e. $\mathcal{A} = 1 - \mathcal{R} - \mathcal{T}$, where $\mathcal{A}$ is the absorption coefficient, $\mathcal{R}$ the reflection coefficient and $\mathcal{T}$ the transmission coefficient. Results are shown in Fig. 4.

It can be seen in Fig. 4 that the absorption and transmission properties of the reference samples can be modified, and depending on the design criteria improved, by adding rigid scatterers. The performance does, however, vary significantly among the studied variants. A mono-layer ⊐ configuration with

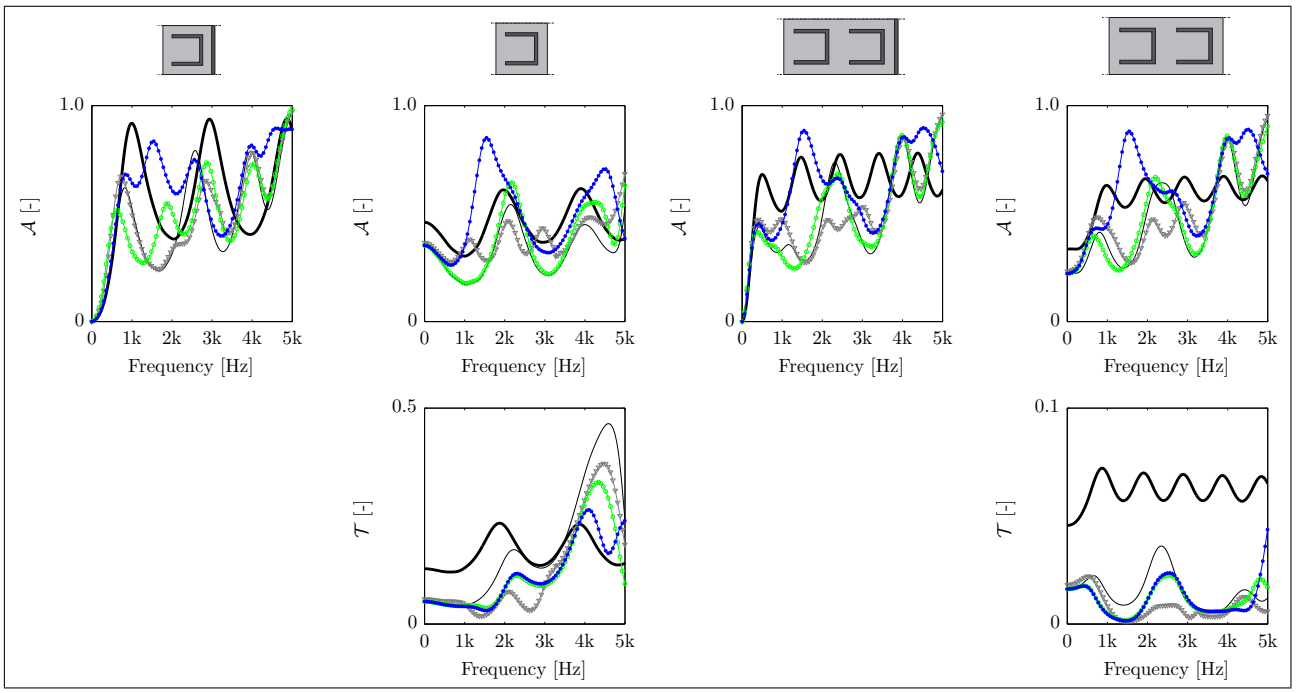

Figure 4. The normal incidence sound absorption $\mathcal{A}$ and transmission loss coefficients $\mathcal{T}$ for a mono (5.25 cm) and double (10.5 cm) layer of porous material, with or without rigid backing. For all plots we have, *thick-black*: reference case without inclusion(s); *thin-black*: $\square$-inclusion(s); *green, open-circles*: $\sqcup$-inclusions; *blue, closed-circles*: $\sqsupset$-inclusions and *grey, down pointing triangle*: $\sqsubset$-inclusions. All inclusion side-lengths are 2.75 cm. The illustrations shown on top are indicative and not true to scale.

rigid backing exhibits improved absorptive properties around the 2 and 4 kHz dips observed in the reference, though at a cost of a reduced peak-absorption. The $\square$, $\sqsubset$ and $\sqcup$ configurations seem less beneficial choices, as the global performance reduced compared to the hard-backed mono-layer reference. The transmission loss of a mono-layer without rigid backing, on the other hand, is increased below 3.5 kHz and decreased above that frequency, for all studied cases. By analysing both $\mathcal{A}$ and $\mathcal{T}$, it can be seen that the effect below 3.5 kHz is due to a combination of increased reflectance (reduced absorption and lower transmittance) and increased absorption. Notice also, the absorption peak at around 1.5 kHz for the $\sqsupset$ configuration, which can be associated to the longitudinal cavity mode in the profile. As a consequence the effect is global and appears in all $\sqsupset$ absorption spectra, regardless of the layer-thickness. Increasing the thickness to a two-layer configuration, the transmittance has been further reduced due to a combination of increased absorption and reflectance. A double layer configuration with rigid backing exhibits approximately the same absorptive properties as the cases without rigid backing, though the overall effect of adding inclusions seems to act negatively on the absorption properties.

4. Insertion loss in a two-dimensional outdoor environment

In the previous section, normal incidence sound absorption and transmission loss characteristics of a 5.25 and 10.5 cm thick layer of porous material, with and without scattering inclusions, has been studied. These calculation results revealed that only a small set of configurations are worth considering for further analysis. As such, we will continue to investigate the insertion loss (IL) spectra of 1 m tall screens for: mono and double layer $\sqsupset$ configurations with rigid backing, and a double layer $\sqsupset$ configuration without rigid backing. In addition, low-height noise barriers without scattering inclusions, as well as acoustically rigid structures having the same cross-sectional area, will be computed. For all cases, the lower-left corner of the barrier is placed in the origin of the domain, and a coherent line-source is located at $(x_s,\, z_s)$ = (-2 m, 0.001 m). The time-variant pressure response is recorded at $(x_r,\, z_r)$ = (5 m, 1.5 m) and $(x_r,\, z_r)$ = (10 m, 1.5 m). Two basic geometrical configurations are considered: (i) the noise barrier with hard ground, and (ii) the noise barrier with hard ground and a car-body cross-section, see Fig 5.

The presence of a scattering body parallel to the barrier will introduce multiple reflections between both objects, and will demonstrate the necessity of having absorbing surfaces for low-height noise barriers. Note that, the car-body is here idealised as a

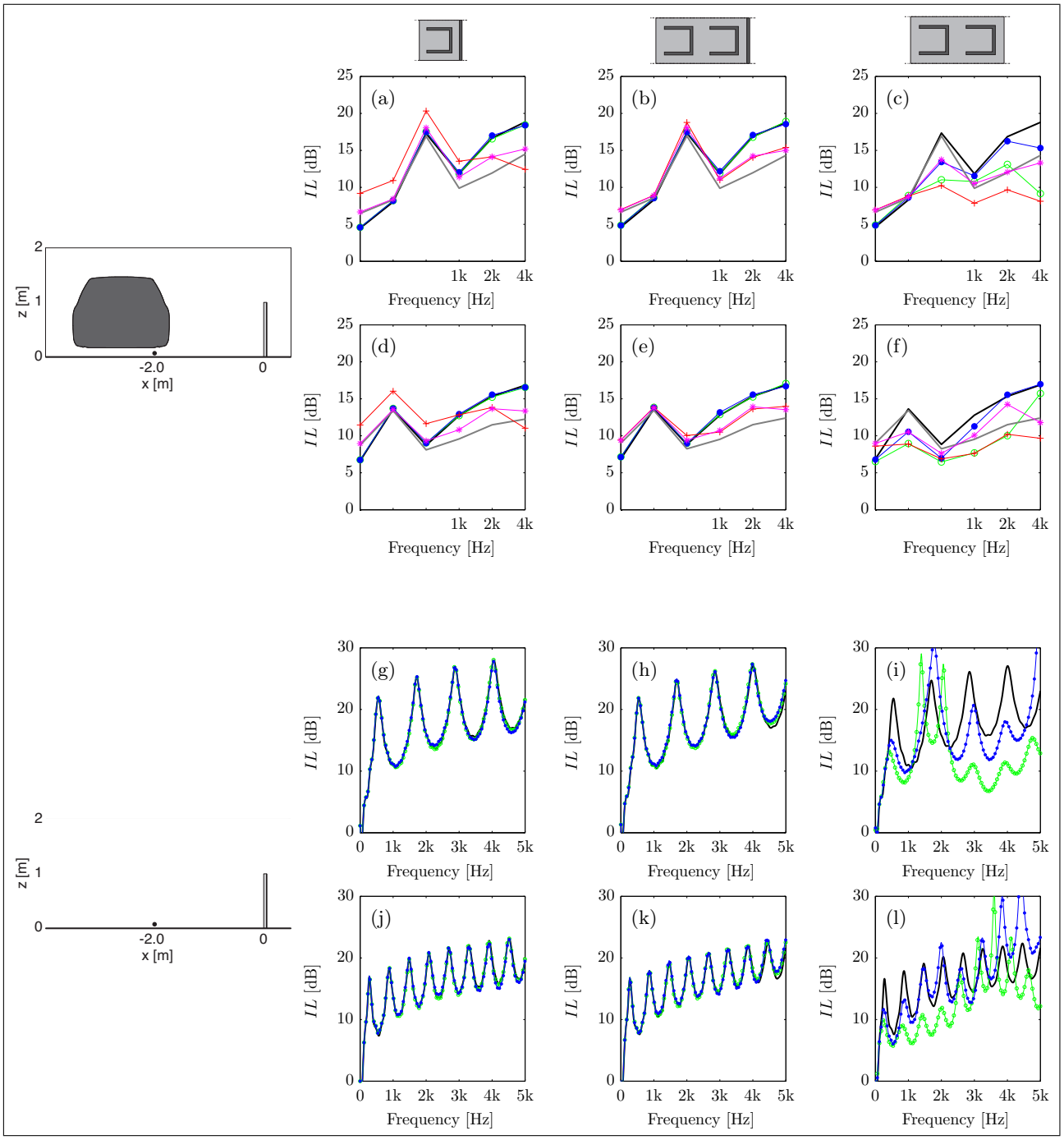

Figure 5. Narrowband and octave-band averaged insertion loss spectra, for a mono (5.25 cm) and double (10.5 cm) layer of porous material, with or without rigid backing. For all subfigures we have, *thick-black*: rigid screen, no car; *thick-grey*: rigid screen, with car; *green, open-circles*: no inclusions, no car; *red, crosses:* no inclusions, with car; *blue, closed-circles*: ⊐-inclusions, no car, and *magenta, asterix*: ⊐-inclusions, with car. (a–c): octave-band averaged IL at $(x_r, z_r) = (10\text{ m}, 1.5\text{ m})$, (d–f): octave-band averaged IL at $(x_r, z_r) = (5\text{ m}, 1.5\text{ m})$, (g–i): narrowband IL at $(x_r, z_r) = (10\text{ m}, 1.5\text{ m})$ and (j–l): narrowband IL at $(x_r, z_r) = (5\text{ m}, 1.5\text{ m})$.

perfectly reflecting two-dimensional cross-section of a Skoda Octavia, where the right-hand side of the body has been offset by 0.27 m with the source. The smallest gap between ground-surface and car body is measured to be 17 cm.

Narrowband IL spectra of various low-height noise barriers in a geometrical configuration without car-body are shown in Fig. 5: g–l. It can be seen that, the barriers with rigid backing are graphically almost indistinguishable for both receiver locations. However, without a rigid backing energy can (partly) propagate through, and significant differences are found. The difference is determined by including scattering units, which introduce multiple scattering effects inside the

porous matrix. As a consequence the transmission is reduced at dedicated frequency intervals. The global noise reducing effect remains, however, worse than the rigid reference barrier, which is better seen in the octave band averaged insertion loss spectra plotted in Fig. 5: c and f.

The influence of the car-body is now discussed in terms of the octave-band averaged insertion loss spectra, for the same receiver locations as introduced previously. It can be seen that the screening effect of a rigid barrier is significantly reduced when considering multiple reflections between car-body and noise barrier. Interchanging a rigid surface with a porous surface has a positive effect on the predicted insertion loss, for all studied cases with a rigid backing. Adding $\sqsupset$ scatterers in a mono-layer matrix with hard backing does improve the high frequency performance in the 4 kHz octave band, though at a cost of a significantly reduced insertion loss below the 2 kHz octave band (compared to the porous barrier without scattering units added).

5. Discussion and Conclusions

An initial study on the reduction of urban road traffic noise using porous low-height noise barriers with scattering inclusions was presented. It has been shown that these structures, either with or without scatterers, are more effective noise reducing devices as compared to acoustically rigid structures, occupying the same cross-sectional area. Especially, when complex geometries giving rise to multiple reflections between e.g. a car and the noise barrier are considered, the improvement is significant. Further research on the optimisation of scattering inclusions, the porous layer, and the influence of more realistic three-dimensional geometries is needed.

Acknowledgement

The research leading to these results has received funding from the European Community's Seventh Framework Programme (FP7/2007-2013) under grant agreement no. 234306, collaborative project HOSANNA, and by the Swedish Governmental Agency for Innovation Systems - VINNOVA - through the national project Urban Acoustic Screens.

References

[1] L. C. Den Boer and A. Schroten. Traffic noise reduction in europe. *Health effects, social costs and technical and policy options to reduce road and rail traffic noise. CE Delft*, 2007.

[2] L. Ding, T. Van Renterghem, and D. Botteldooren. Estimating the effect of semi-transparent low-height road traffic noise barriers with ultra weak variational formulation. *Acta Acustica united with Acustica*, 97(3):391–402, May 2011.

[3] J.-P. Groby, O. Dazel, A. Duclos, L. Boeckx, and L. Kelders. Enhancing the absorption coefficient of a backed rigid frame porous layer by embedding circular periodic inclusions. *The Journal of the Acoustical Society of America*, 130(6):3771–3780, 2011.

[4] J.-P. Groby, A. Wirgin, L. De Ryck, W. Lauriks, R. P. Gilbert, and Y. S. Xu. Acoustic response of a rigid-frame porous medium plate with a periodic set of inclusions. *The Journal of the Acoustical Society of America*, 126(2):685, 2009.

[5] F. Koussa, J. Defrance, P. Jean, and P. Blanc-Benon. Acoustic performance of gabions noise barriers: Numerical and experimental approaches. *Applied Acoustics*, 74(1):189–197, Jan. 2013.

[6] C. Lagarrigue, J. P. Groby, V. Tournat, O. Dazel, and O. Umnova. Absorption of sound by porous layers with embedded periodic arrays of resonant inclusions. *The Journal of the Acoustical Society of America*, 134(6):4670–4680, 2013.

[7] B. Nennig, Y. Renou, J.-P. Groby, and Y. Aurégan. A mode matching approach for modeling two dimensional porous grating with infinitely rigid or soft inclusions. *The Journal of the Acoustical Society of America*, 131(5):3841–3852, 2012.

[8] V. E. Ostashev, D. K. Wilson, L. Liu, D. F. Aldridge, N. P. Symons, and D. Marlin. Equations for finite-difference, time-domain simulation of sound propagation in moving inhomogeneous media and numerical implementation. *The Journal of the Acoustical Society of America*, 117(2):503, 2005.

[9] P. J. Thorsson. Optimisation of low-height noise barriers using the equivalent sources method. *Acta Acustica united with Acustica*, 86(5):811–820, 2000.

[10] T. Van Renterghem. *The finite-difference time-domain method for simulation of sound propagation in a moving medium.* PhD thesis, University of Ghent, 2003.

[11] X. Yuan, D. Borup, J. W. Wiskin, M. Berggren, R. Eidens, and S. A. Johnson. Formulation and validation of berenger's PML absorbing boundary for the FDTD simulation of acoustic scattering. *Ultrasonics, Ferroelectrics and Frequency Control, IEEE Transactions on*, 44(4):816–822, 1997.

[12] C. Zwikker and C. Kosten. *Sound Absorbing Materials.* Elsevier, New York, 1949.